




Research Article

Direct Electron Transfer from Upconversion Graphene Quantum Dots to TiO₂ Enabling Infrared Light-Driven Overall Water Splitting

Dongmei Jia,¹ Xiaoyu Li,¹ Qianqian Chi,¹ Jingxiang Low,² Ping Deng,¹ Wenbo Wu,¹ Yikang Wang,¹ Kaili Zhu,¹ Wenhao Li,¹ Mengqiu Xu,¹ Xudong Xu,¹ Gan Jia,¹ Wei Ye ¹, Peng Gao ¹ and Yujie Xiong ²

¹College of Material, Chemistry and Chemical Engineering, Hangzhou Normal University, Hangzhou, Zhejiang 311121, China

²School of Chemistry and Materials Science, University of Science and Technology of China, Hefei, Anhui 230026, China

Correspondence should be addressed to Wei Ye; yewei@hznu.edu.cn, Peng Gao; gaopeng@hrbeu.edu.cn, and Yujie Xiong; yjxiong@ustc.edu.cn

Received 13 January 2022; Accepted 17 March 2022; Published 13 April 2022

Copyright © 2022 Dongmei Jia et al. Exclusive Licensee Science and Technology Review Publishing House. Distributed under a Creative Commons Attribution License (CC BY 4.0).

Utilization of infrared light in photocatalytic water splitting is highly important yet challenging given its large proportion in sunlight. Although upconversion material may photogenerate electrons with sufficient energy, the electron transfer between upconversion material and semiconductor is inefficient limiting overall photocatalytic performance. In this work, a TiO₂/graphene quantum dot (GQD) hybrid system has been designed with intimate interface, which enables highly efficient transfer of photogenerated electrons from GQDs to TiO₂. The designed hybrid material with high photogenerated electron density displays photocatalytic activity under infrared light (20 mW cm⁻²) for overall water splitting (H₂: 60.4 μmol g_{cat.}⁻¹ h⁻¹ and O₂: 30.0 μmol g_{cat.}⁻¹ h⁻¹). With infrared light well harnessed, the system offers a solar-to-hydrogen (STH) efficiency of 0.80% in full solar spectrum. This work provides new insight into harnessing charge transfer between upconversion materials and semiconductor photocatalysts and opens a new avenue for designing photocatalysts toward working under infrared light.

1. Introduction

The sun provides 173,000 TW energy every year, 9,000 times more than the annual world energy consumption. While the energy proportion of infrared (IR) light exceeds 50% in sunlight, the IR light has not been efficiently utilized for solar-to-chemical energy conversion by now due to the lack of related ideal materials to photogenerate electrons with sufficient energy and density. As a typical example, solar-driven water splitting, which can produce hydrogen with the energy density of 141.9 MJ/kg, possesses a 0.5 eV overpotential and requires the energy input of at least 1.8 eV corresponding to the photons at <688 nm. To implement IR or near-IR (NIR) (780~2526 nm) light in water splitting, two main strategies have been developed including localized surface plasmon resonance- (LSPR-) induced hot electron injection and photon upconversion-induced electron injection. For

instance, a CdS/Cu₇S₄ photocatalyst was employed for water splitting, in which LSPR-induced hot electrons from Cu₇S₄ were injected into CdS under NIR illumination (>800 nm) [1–3]. Similarly, other photocatalysts were demonstrated based on Au nanostructures with LSPR band in IR spectral region [4–6]. In parallel, photon upconversion is another strategy for utilizing NIR or IR light in solar energy storage and conversion. For instance, core-shell Pt@MOF/Au composites can convert NIR light to UV and visible light, driving photocatalytic hydrogen production under NIR irradiation [7]. Such an (N)IR-driven photocatalysis was also achieved by rare-earth upconversion materials [8–12]. Nevertheless, the energy conversion performance of the existing systems using NIR or IR light is unsatisfactory through the two strategies. The performance of two strategies relies on plasmonic hot electron generation or photon upconversion and, more importantly, their charge or energy transfer to semiconductor

photocatalyst. As a matter of fact, the efficiency of these fundamental processes is relatively low, constituting the obstacle for overall performance.

Recently, graphene quantum dots (GQDs), as a class of zero-dimensional nanomaterials based on graphene, have attracted extensive attention owing to their advantages including low toxicity, high electron mobility ($10,000\text{ cm}^2\text{ s}^{-1}$), high carrier concentration ($1,013\text{ cm}^{-2}$), low cytotoxicity, and facile surface grafting [13–16]. In addition, the quantum confinement and edge effect of GQDs endow them with more active sites [17, 18], wide optical absorption range [19], tunable band structure, and (N)IR upconversion photoluminescence (PL) behavior [20]. In particular, a previous work has demonstrated that the energy difference between excitation light and emission light in the upconversion process is close to 1.1 eV because the p electrons are excited to a high-energy state (e.g., lowest unoccupied molecular orbital, LUMO) and then transition back to the s orbital [21]. We envision that such an upconversion material should be an ideal candidate for forming intimate interface with semiconductor given its facile surface chemistry, which would allow the direct transfer of multiphoton-generated electrons from upconversion GQDs to semiconductor photocatalyst (instead of emitting higher-energy photons) toward (N)IR-driven chemical reactions. Certainly, this opportunity based on upconversion GQDs remains largely unexplored in photocatalysis.

In this work, we demonstrate the concept that the electrons NIR-generated in GQDs through a multiphoton process can be directly transferred to semiconductor toward photocatalytic overall water splitting. As a model system, the surface of 2–3 layered GQDs is modified by reduction treatment and forms intimate bonding with TiO_2 nanotube photocatalyst, enabling efficient interfacial electron transfer. As a result, the GQDs can offer energy-sufficient electrons under IR irradiation for the photocatalyst to drive water splitting. While the composite displays a strong light absorption from UV region to IR region, the IR activity enhances the photocatalytic performance of overall water splitting to the solar-to-hydrogen (STH) efficiency of 0.80%.

2. Results

The GQDs are prepared through evolution from glucose and are further treated to remove surface oxygen-containing groups through reduction with NaBH_4 , producing r-GQDs. To demonstrate the importance of interface to charge transfer, the GQDs and r-GQDs with different surface conditions are both used for integration with TiO_2 nanotubes through the same hydrothermal process. Figure 1(a) shows the XRD patterns of pure TiO_2 , TiO_2/GQDs , and $\text{TiO}_2/\text{r-GQDs}$ composites. After integrated with TiO_2 , the intensity of the peaks corresponding to TiO_2 is evidently reduced. This suggests that the crystallinity of TiO_2 is lowered by the addition of GQDs (r-GQDs) or/and the TiO_2 is largely covered by the GQDs (r-GQDs). In addition, the average grain size of TiO_2 is calculated to be about 12 nm using Scherrer formula according to its XRD pattern. To gain surface information, Fourier transform infrared spectroscopy (FT-IR) is employed

to characterize the samples. As shown in Figure 1(b), the oxygen groups such as OH ($\sim 3400\text{ cm}^{-1}$) and C=O ($\sim 1400\text{ cm}^{-1}$) in GQDs are obviously reduced after NaBH_4 reduction. In the meantime, it creates abundant dangling bonds of carbon, which then are bonded with oxygen atoms in TiO_2 [23, 24]. As a result, the Ti-O-C chemical bonds at 950 cm^{-1} are observed in $\text{TiO}_2/\text{r-GQDs}$ [25–27].

The formation of such Ti-O-C chemical bonds is also confirmed by X-ray photoelectron spectroscopy (XPS). As shown in Figure 1(c), the XPS survey spectrum of $\text{TiO}_2/\text{r-GQDs}$ composite demonstrates the existence of O, Ti, and C elements. The C1s peaks at 284.6 eV, 285.6 eV, and 288.7 eV are attributed to C-C, C=C and C-O-Ti bonds, respectively (Figure 1(d)) [28]. The Ti-O-C bond is also detected by the peaks at 531.6 eV of O1s (Figure 1(e)) and 457.8 eV of Ti2p (Figure 1(f)) XPS spectra [21]. In comparison, the peaks for Ti-O-C bond have not been found for TiO_2 and TiO_2/GQDs (fig. S1). As such, the peak intensity change of TiO_2 in XRD should also be partially associated with the formation of Ti-O-C chemical bonding between TiO_2 and r-GQDs. This chemical bonding at the interface of $\text{TiO}_2/\text{r-GQDs}$ surely will facilitate the interfacial electron transfer by lowering the potential barrier between TiO_2 and r-GQDs [29, 30]. It is known that most composites are formed without intimate connection between two different components to leave gaps or defects at the interface, which forms a depletion layer to hinder the charge transfer to a large extent. A chemically bonded interface in the composite undoubtedly provides a better charge transfer path and enables efficient charge transfer from interface to surface.

To reveal the morphologies and microstructures, the samples are examined by transmission electron microscopy (TEM). Figure 2(a) shows that the as-prepared GQDs have the size of about 2–3 nm. As indicated by Raman spectroscopy (Figure 2(b) and fig. S2), both GQDs and r-GQDs are 2–3 layered thick. Meanwhile, the TiO_2 nanotubes that are used for integration with GQDs and r-GQDs have a width of $\sim 7.4\text{ nm}$ and a length of several micrometers (Figure 2(c)). High-resolution TEM (HRTEM, Figure 2(d)) reveals that the TiO_2 nanotubes possess relatively smooth surface. Raman spectroscopy also confirms that the TiO_2 nanotubes are of anatase phase (fig. S3). After uniformly integrated with GQDs or r-GQDs, the one-dimensional morphology is well maintained as indicated by TEM and elemental mapping (Figures 2(e)–2(i)). Despite the remained nanotubes, the samples display interesting characteristics in Brunauer-Emmett-Teller (BET) surface areas (the insets of Figures 2(c), 2(e), and 2(g)). The TiO_2 nanotubes and TiO_2/GQDs exhibit similar BET surface areas ($93.8\text{ m}^2/\text{g}$ and $97.2\text{ m}^2/\text{g}$) and pore size distributions (fig. S4). However, the BET area of $\text{TiO}_2/\text{r-GQDs}$ reaches up to $275.3\text{ m}^2/\text{g}$ (Figure 2(g)). Most likely, this feature is associated with the Ti-O-C chemical bonding between TiO_2 and r-GQDs, which induces the electronegativity change in both TiO_2 and r-GQDs promoting N_2 polarization and adsorption. The integrated composite structure of $\text{TiO}_2/\text{r-GQDs}$ has also been resolved by HRTEM (Figures 2(j)–2(l)), showing that hexangular r-GQDs are loaded on the surface of TiO_2 nanotubes. Aberration-

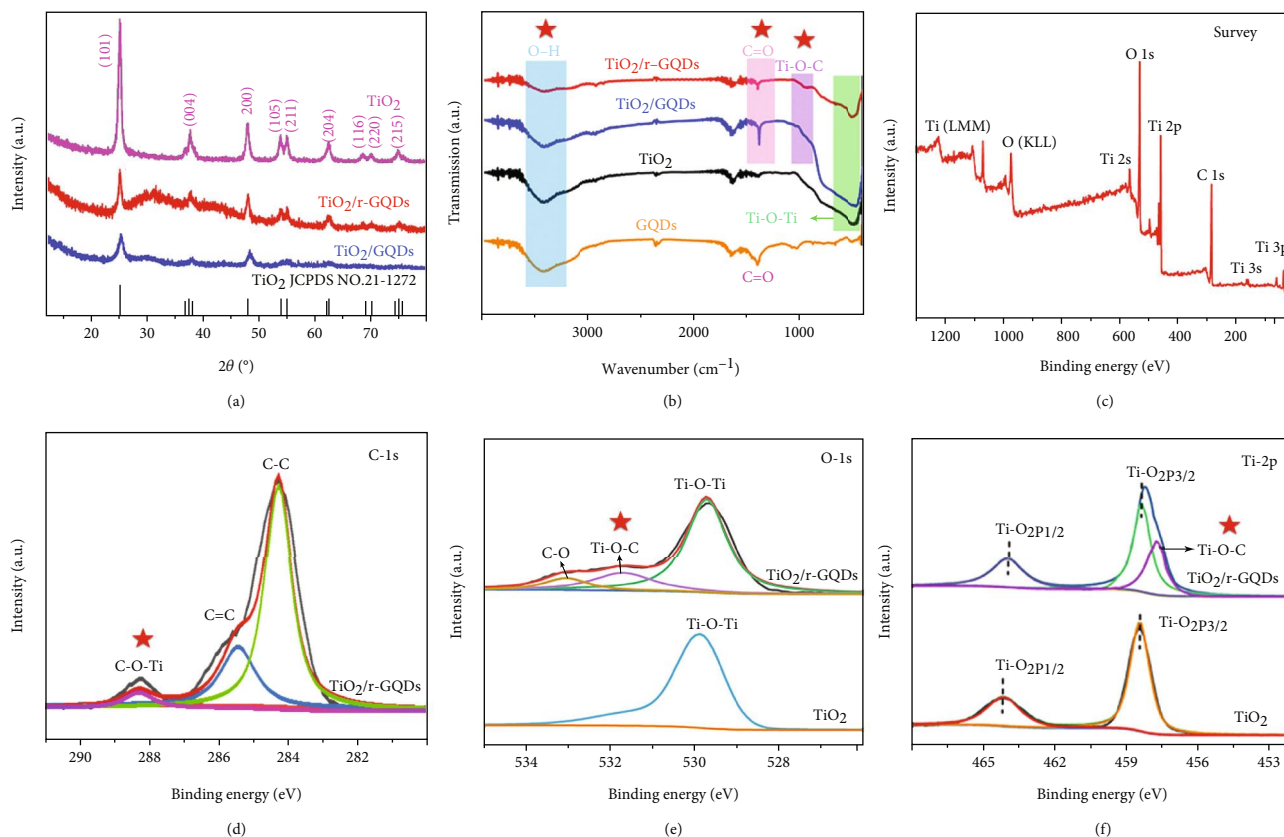


FIGURE 1: (a) XRD patterns and (b) FT-IR spectra of the obtained GQDs, TiO₂, TiO₂/GQDs, and TiO₂/r-GQDs. XPS spectra of the TiO₂ and TiO₂/r-GQDs: (c) survey, (d) C1s, (e) O1s, and (f) Ti2p.

corrected TEM (AC-TEM, Figures 2(m) and 2(n)) further confirms the existence of r-GQDs and TiO₂ at atomic resolution.

The addition of GQDs and r-GQDs broadens the light absorption of TiO₂ nanotubes to visible region as shown in fig. S5. To determine band structures, valence-band spectra are measured by XPS (Figure 2(o)). As depicted in Figure 2(p), GQDs lower the conduction band (CB) edge from -0.18 eV to +0.21 eV, which is unfavorable for hydrogen evolution through water splitting. However, r-GQDs can elevate the CB and valence band (VB) edges to -0.26 eV and +2.38 eV, respectively, which enable overall water splitting for hydrogen and oxygen production simultaneously. This highlights that the surface modification on GQDs has a significant impact on band structures, which may in turn alter charge dynamics.

To look into charge dynamics, we closely examine the PL behavior of samples. It is known that the capture centers for excitons are formed by surface oxidation, leading to surface-state-related fluorescence [31]. As shown in Figure 3(a), after reduction of GQDs, the PL emission of graphene quantum dots exhibits an obvious blue-shift from 433 to 418. This observation is similar to the finding in literature that the bandgap is widened as a decreasing number of oxygen atoms are present in the structure, resulting in a PL blue-shift [32]. More importantly, multiphoton upconversion-induced emissions at 546 nm and 663 nm are detected for the GQD-based samples under a 980 nm IR light excitation as

shown in Figure 3(b). This upconverted PL property of GQDs should be attributed to the multiphoton active process similar to the previously reported carbon dots [33], indicating that GQDs should be a powerful energy-transfer component in photocatalyst design. The unchanged emission positions between GQDs and r-GQDs demonstrate that the emission should originate from carbon core rather than surface state. After GQDs are anchored on TiO₂, the sample displays the strengthened upconverted PL emission, suggesting that more active electrons are formed on surface. The time-resolved PL spectra (Figure 3(c)) show that the average PL lifetimes of r-GQDs, TiO₂/GQDs, and TiO₂/r-GQDs are 0.3 ns, 1.17 ns, and 9.06 ns, respectively, proving that the photogenerated electrons of r-GQDs can be timely extracted by coupling with TiO₂.

This argument is also supported by photocurrent measurements as displayed in Figure 3(d). The photocurrents by TiO₂/r-GQDs are dramatically higher than those by TiO₂/GQDs and TiO₂, demonstrating that charge separation and transfer are better harnessed in TiO₂/r-GQDs. As a supplementary experiment, electrochemical impedance spectroscopy (EIS) measurements (Figures 3(e) and 3(f)) are carried out at a 4 kHz frequency in dark and under 420 nm illumination. It shows that the arc radius under light irradiation is smaller than that in dark. As compared with TiO₂ and TiO₂/GQDs, the Nyquist plot of TiO₂/r-GQDs displays a substantially smaller radius under irradiation, which further

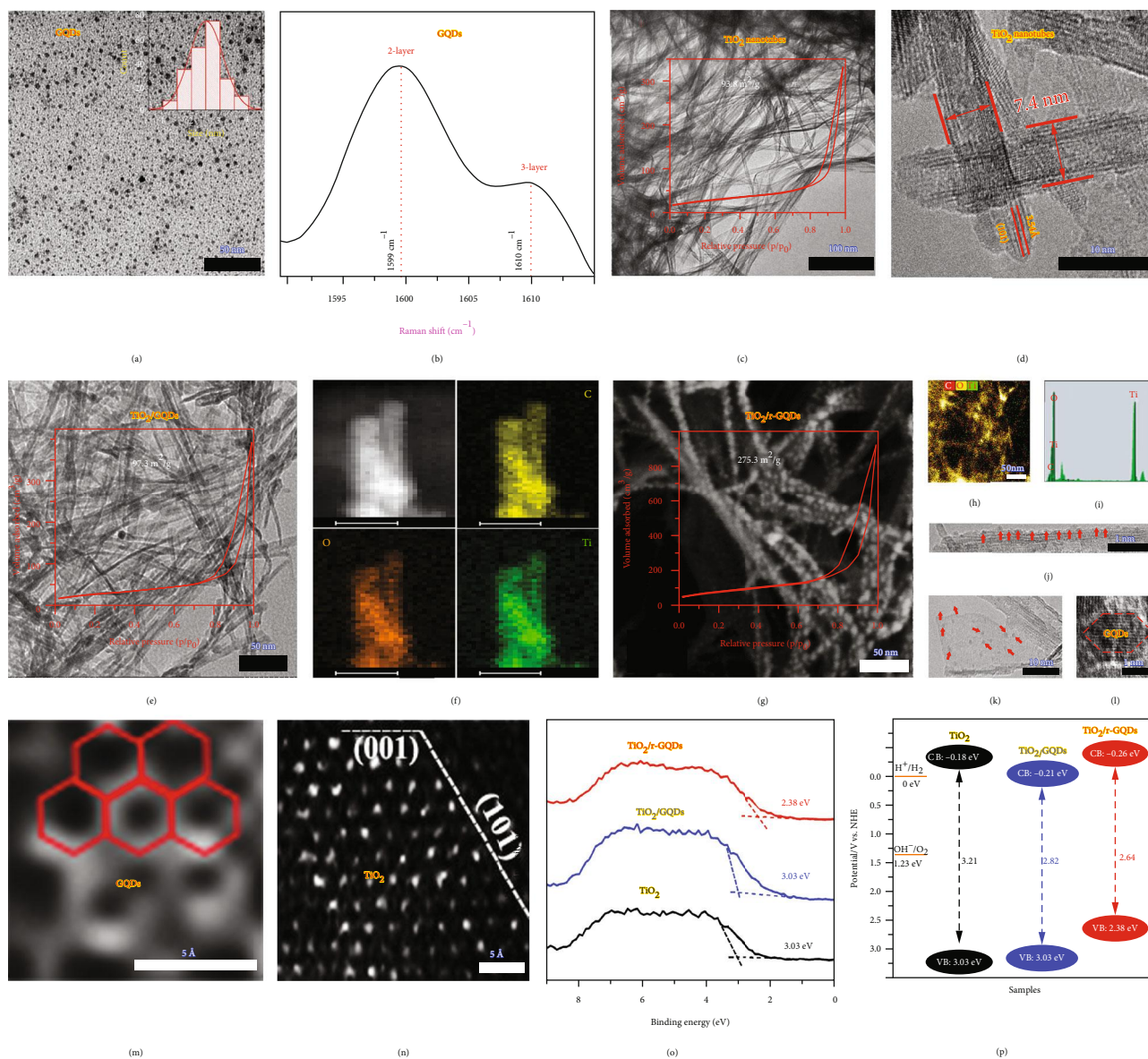


FIGURE 2: Morphology and microstructure characterization of the samples. (a) TEM image and (b) Raman spectrum of the obtained GQDs. The inset of (a) shows the size distribution. (c) TEM image and (d) HRTEM images of the obtained TiO₂ nanotubes. The inset of (c) shows the BET result. (e) TEM image and (f) elemental mapping profiles of the obtained TiO₂/GQDs (scale bars are 10 nm). The inset of (e) shows the BET result. (g) TEM image, (h) elemental mapping profile, (i) EDX spectrum, (j-l) HRTEM images, and (m, n) AC-TEM images of the obtained TiO₂/r-GQDs. (o) Valence-band spectra measured by XPS and (p) band structures of the three samples.

proves the improved separation efficiency of electron-hole pairs in TiO₂/r-GQDs [34]. The enhanced charge separation in TiO₂/r-GQDs is also demonstrated by surface photovoltage spectroscopy (SPS) (fig. S6). It is known that distinct SPS signal can reflect the enhanced separation rate of photo-induced charge pairs [35]. Among these features, the high conductivity and strong electron transfer ability of r-GQDs facilitate the access to electrons and the electron diffusion process, effectively improving the charge transfer in the photocatalyst. Taken together, the r-GQDs possess the upconversion properties for harvesting IR photons and the electronic properties for efficient charge transfer, which should be a good candidate to offer high photocatalytic activity.

We are now in a position to evaluate the photocatalytic overall water splitting performance of the samples. The measurements are first carried out under ultraviolet light without the addition of precious metal cocatalyst and sacrificial agent. As shown in Figure 3(g), pure TiO₂ and TiO₂/GQDs do not have the ability for overall water splitting due to their mismatched energy level structure or unsuitable bandgap (Figure 2(p)). In contrast, TiO₂/r-GQDs show excellent photocatalytic performance for overall water splitting under UV light with the H₂ production rate of 358.8 μmol g_{cat.}⁻¹ h⁻¹ and the O₂ production rate of 175.9 μmol g_{cat.}⁻¹ h⁻¹. More importantly, TiO₂/r-GQDs also exhibit photocatalytic activity for overall water splitting under IR light. As shown in

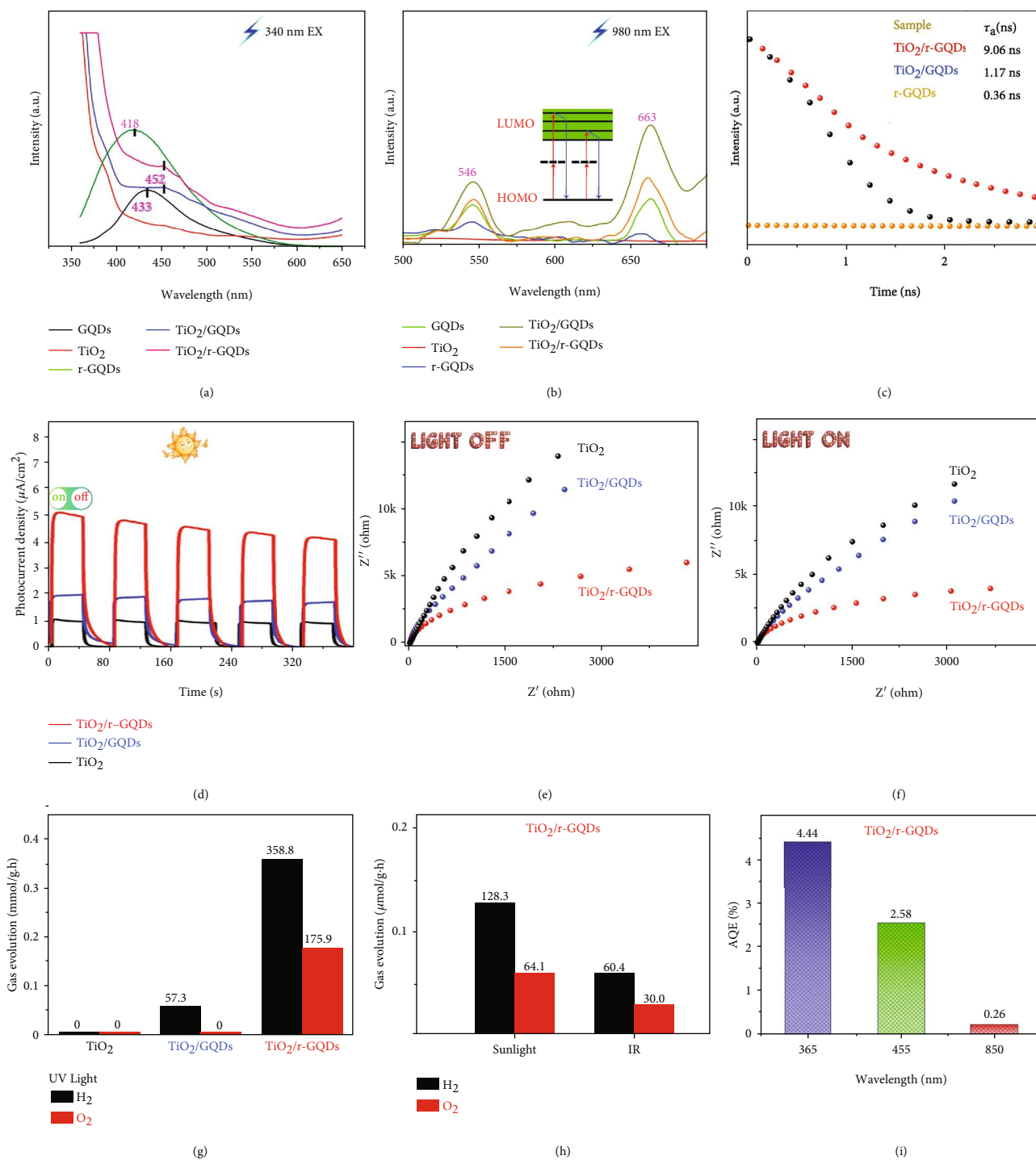


FIGURE 3: Charge dynamics behavior and photocatalytic performance. PL spectra of the samples with (a) 340 nm and (b) 980 nm excitation. (c) Fluorescence lifetime spectra, (d) transient photocurrent spectra, and (e, f) electrochemical impedance spectra of the TiO₂, TiO₂/GQDs, and TiO₂/r-GQDs. (g, h) Photocatalytic water splitting performance (UV light: 100 mW cm⁻²; sunlight: 100 mW cm⁻²; and IR light: 20 mW cm⁻²). (i) AQE values of TiO₂/r-GQDs under different illumination wavelengths.

Figure 3(h), the photocatalyst offers the values of H₂ (60.4 μmol g_{cat.}⁻¹ h⁻¹) and O₂ (30.0 μmol g_{cat.}⁻¹ h⁻¹) production under IR light (>800 nm, 20 mW cm⁻²). As such, the H₂/O₂ production rates of 128.3/64.1 μmol g_{cat.}⁻¹ h⁻¹ are achieved in full spectrum (100 mW cm⁻²). To better assess the overall performance, the STH efficiency is determined

to be 0.80%. In addition, the apparent quantum efficiency (AQE) of TiO₂/r-GQDs under different illustration wavelengths (365 nm: 61 mW cm⁻², 455 nm: 45 mW cm⁻², and 850 nm: 15 mW cm⁻²) is measured, respectively, as shown in Figure 3(i). The sample displays a 0.26% AQE even under 850 nm infrared light, which further confirms its

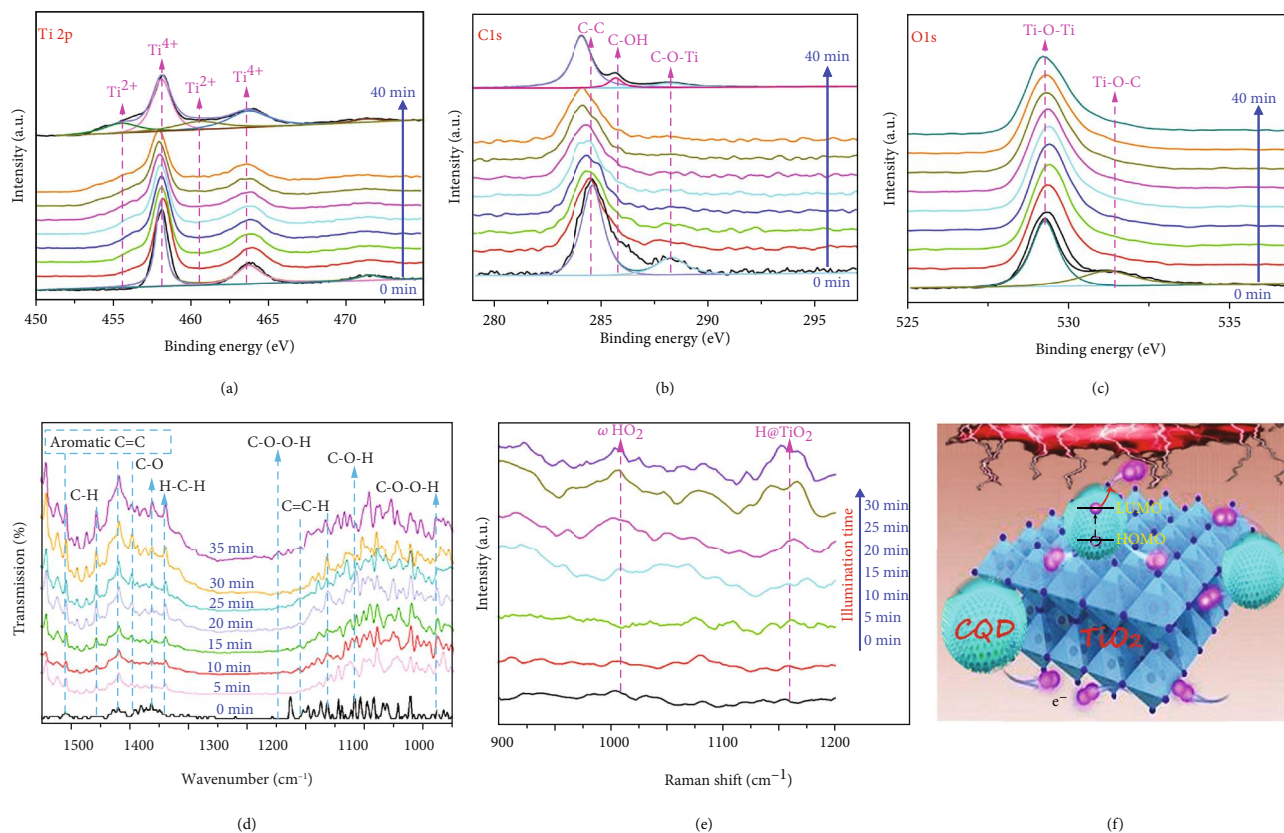


FIGURE 4: Electron transfer from r-GQDs to TiO_2 investigated by (a–c) in situ XPS, (d) in situ FT-IR, and (e) in situ Raman measurements. (f) Illustration of the electron transfer process in TiO_2 /r-GQDs.

outstanding ability for overall water splitting. The TiO_2 /r-GQD photocatalyst also shows high stability in cycling tests as shown in fig. S7-S9.

Upon recognizing the performance, a question naturally arises how the upconversion r-GQDs participate in water splitting after harvesting IR light. To decode the mechanism, we employ in situ XPS to characterize the sample with trace water. As shown in Figure 4(a), the peaks located at 458.0 and 460.6, 455.3, and 463.7 eV are attributed to the Ti^{4+} and Ti^{2+} oxidation states, respectively. The peaks belonging to Ti^{2+} show an increasing trend with the extension of irradiation time. At the same time, the common Ti^{3+} peaks, such as that around 457.0 eV for $\text{Ti}2p_{1/2}$, are not distinct [36, 37]. In comparison, only Ti^{3+} is observed for TiO_2 -based photocatalysts under light irradiation [38, 39]. This indicates that the electrons generated from the upconversion of r-GQDs can be directly transferred to TiO_2 . In addition, a shift of C1s peaks toward lower binding energies is observed in Figure 4(b), which should be due to the lowered electron density in carbon atoms after the electron transfer process and further demonstrates the electron transfer from r-GQDs to TiO_2 under illumination. In the meantime, the O1s peaks assigned to TiO_2 and Ti-O-C (Figure 4(c)) are unchanged. The water splitting process is also characterized by in situ FT-IR spectroscopy. As shown in Figure 4(d), once the light is turned on, the peaks corresponding to C-H (1458 cm^{-1}), C-O stretching in carboxyl (1364 cm^{-1}), H-C-H (1340 cm^{-1}), and C-O-O-H (1148 cm^{-1} and 878 cm^{-1}) are

gradually strengthened [40, 41]. The appearance of these transient oxygen-containing species confirms the fact that the oxygen evolution reaction (OER) takes place on CQDs. Simultaneously, the crucial C-O-O-H intermediate detected in water splitting points out a single-site process of OER [36], which is known as the rate-limiting step. In this single-site process, firstly a -OH is bonded with carbon atom of CQD and then loses its hydrogen atom to form a C-O species. Further another -OH is added on C-O for -COOH formation, which finally releases an O_2 molecule. In addition, the peaks attributed to Ti-H are also found in the measurement (Figure 4(e) and fig. S10), suggesting that hydrogen is produced at the Ti sites in TiO_2 [42, 43]. The efficient transfer of upconversion-generated electrons from r-GQDs to the Ti sites in TiO_2 is responsible for the IR-driven overall water splitting as illustrated in Figure 4(f).

It should be noted that such efficient transfer of upconversion electrons can also trigger photocatalytic CO_2 reduction with IR light. As shown in fig. S11-15, the TiO_2 /r-GQD sample shows $19.49\text{ }\mu\text{mol g}_{\text{cat}}^{-1}\text{ h}^{-1}$ CO and $3.13\text{ }\mu\text{mol g}_{\text{cat}}^{-1}\text{ h}^{-1}$ CH_4 production rates under full-spectrum light (100 mW cm^{-2}) as well as $0.45\text{ }\mu\text{mol g}_{\text{cat}}^{-1}\text{ h}^{-1}$ CO and $0.03\text{ }\mu\text{mol g}_{\text{cat}}^{-1}\text{ h}^{-1}$ CH_4 production rates under weak IR light ($>800\text{ nm}$, 20 mW cm^{-2}).

3. Discussion

In summary, reduced graphene quantum dots are integrated with TiO_2 photocatalyst by forming intimate interface,

allowing the direct transfer of multiphoton-generated electrons from r-GQDs to TiO_2 toward IR-driven photocatalysis. The high electron density induced by such a direct electron transfer invests the sample with prominent photocatalytic abilities under infrared light for not only overall water splitting but also CO_2 reduction. Remarkably, the designed hybrid material achieves photocatalytic overall water splitting for H_2 at $60.4 \mu\text{mol g}_{\text{cat.}}^{-1} \text{h}^{-1}$ and O_2 at $30.0 \mu\text{mol g}_{\text{cat.}}^{-1} \text{h}^{-1}$ under infrared light ($>800 \text{ nm}$, 20 mW cm^{-2}). Such an IR activity makes an important contribution to the STH of 0.80%. This work provides new insights into photocatalyst design for harnessing low-energy photons.

4. Materials and Methods

4.1. Preparation of TiO_2 Nanotubes. All the chemicals were of analytical grade. TiO_2 nanotubes were synthesized using an alkaline hydrothermal process according to the literature [22].

4.2. Preparation of GQDs and r-GQDs. Glucose was dispersed in 40 mL pure water. The solution was stirred in a magnetic stirrer for 10 min, then transferred to a Teflon lined autoclave (50 mL), and heated at 190°C for 3 h. After the reaction, the autoclave was naturally cooled to room temperature. The brown solution was centrifuged for 20 min to remove the precipitate and retain the supernatant, namely, GQDs. The aqueous suspension of GQDs (0.1–1 mg/mL) was added with 50 mg NaBH_4 , and the reaction was under stirring at room temperature for 4 h. The resulted product was named as r-GQDs.

4.3. Preparation of TiO_2/GQDs and $\text{TiO}_2/\text{r-GQDs}$. The TiO_2/GQDs or $\text{TiO}_2/\text{r-GQD}$ composites were obtained by the hydrothermal method. 0.2 g TiO_2 and 40 mL GQDs or r-GQD suspension were mixed. The mixture was continuously stirred at room temperature for 4 h to obtain a uniform suspension. TiO_2/GQDs or $\text{TiO}_2/\text{r-GQD}$ was collected by centrifugation, washed three times with distilled water, and dried in vacuum overnight at 60°C .

Data Availability

All data needed to evaluate the conclusions in the paper are present in the paper and the Supplementary Materials. Additional data related to this paper may be requested from the authors.

Conflicts of Interest

The authors declare that there is no conflict of interest regarding the publication of this article.

Authors' Contributions

P. Gao, D. M. Jia, and Q. Q. Chi conceived the XPS experiments; D. M. Jia carried out the PL, in situ FT-IR, and in situ XPS measurements. J. X. Low analyzed the XRD data. P. Deng and Y. K. Wang conducted the SEM and EDX mea-

surements. W. B. Wu and K. L. Zhu analyzed the TEM measurements and supervised the optical measurements. X. D. Xu, G. Jia, and M. Q. Xu analyzed and interpreted the HRTEM. P. Gao, W. Ye, and Y. J. Xiong supervised the research. All authors have seen the paper, agree to its content, and approve submission. Dongmei Jia, Xiaoyu Li, and Qianqian Chi contributed equally to this work.

Acknowledgments

This work was supported by the Natural Science Foundation of China (51902077 and 21725102), Zhejiang Provincial Natural Science Foundation (LY18E020010 and LQ19B010001), Zhejiang Province “Ten Thousand People Plan” (2018R52015), Pandeng Plan Foundation of Hangzhou Normal University for Youth Scholars of Materials, Chemistry and Chemical Engineering, Agricultural and Social Development Program Project (2020ZDSJ0712) of Hangzhou Science and Technology Bureau of Zhejiang Province, general items of Zhejiang Provincial Department of Education (Y201840068), and Visiting Scholar Development Project of Department of Education of Zhejiang Provincial (FX2019043).

Supplementary Materials

Figure S1: XPS spectra of TiO_2/GQDs . Figure S2: Raman spectrum of r-GQDs. Figure S3: Raman spectrum of TiO_2 . Figure S4: pore size distributions of TiO_2/GQDs and $\text{TiO}_2/\text{r-GQDs}$. Figure S5: UV-vis reflectance spectra and optical bandgaps. Figure S6: SPV spectra. Figure S7: time-dependent IR light-driven photocatalytic water splitting by $\text{TiO}_2/\text{r-GQDs}$. Figure S8: cycling IR light-driven photocatalytic water splitting by $\text{TiO}_2/\text{r-GQDs}$. Figure S9: TEM image of $\text{TiO}_2/\text{r-GQDs}$ after photocatalytic water splitting. Figure S10: in situ FT-IR spectra. Figure S11: time-dependent simulated sunlight-driven photocatalytic CO_2 reduction by $\text{TiO}_2/\text{r-GQDs}$. Figure S12: cycling simulated sunlight-driven photocatalytic CO_2 reduction by $\text{TiO}_2/\text{r-GQDs}$. Figure S13: gas chromatography for CO and CH_4 generation. Figure S14: time-dependent IR light-driven photocatalytic CO_2 reduction by $\text{TiO}_2/\text{r-GQDs}$. Figure S15: cycling IR light-driven photocatalytic CO_2 reduction by $\text{TiO}_2/\text{r-GQDs}$. (*Supplementary Materials*)

References

- [1] Z. Lian, M. Sakamoto, J. Vequizo et al., “Plasmonic p-n junction for infrared light to chemical energy conversion,” *Journal of the American Chemical Society*, vol. 141, pp. 2446–2450, 2019.
- [2] Y. C. Pu, G. Wang, K. D. Chang et al., “Au nanostructure-decorated TiO_2 nanowires exhibiting photoactivity across entire UV-visible region for photoelectrochemical water splitting,” *Nano Letters*, vol. 13, no. 8, pp. 3817–3823, 2013.
- [3] B. Tian, Y. Wu, and G. Lu, “Metal-free plasmonic boron phosphide/graphitic carbon nitride with core-shell structure photocatalysts for overall water splitting,” *Applied Catalysis B*, vol. 280, article 119410, 2021.

- [4] L. Liu, S. Ouyang, and J. Ye, "Gold-nanorod-photosensitized titanium dioxide with wide-range visible-light harvesting based on localized surface plasmon resonance," *Angewandte Chemie International Edition*, vol. 52, no. 26, pp. 6689–6693, 2013.
- [5] Z. Zheng, T. Tachikawa, and T. Majima, "Single-particle study of Pt-modified Au nanorods for plasmon-enhanced hydrogen generation in visible to near-infrared region," *Journal of the American Chemical Society*, vol. 136, no. 19, pp. 6870–6873, 2014.
- [6] Y. C. Chen, Y. K. Hsu, R. Popescu, D. Gerthsen, Y. G. Lin, and C. Feldmann, "Au@Nb@H_x K_{1-x}NbO₃ nanopods with near-infrared active plasmonic hot-electron injection for water splitting," *Nature Communications*, vol. 9, no. 1, p. 232, 2018.
- [7] D. Li, S. H. Yu, and H. L. Jiang, "From UV to near-infrared light-responsive metal-organic framework composites: plasmon and upconversion enhanced photocatalysis," *Advanced Materials*, vol. 30, no. 27, article 1707377, 2018.
- [8] W. Gao, Y. Wu, and G. Lu, "980 nm NIR light driven overall water splitting over a combined CdS-RGO-NaYF₄Yb³⁺/Er³⁺ photocatalyst," *Catalysis Science & Technology*, vol. 10, no. 8, pp. 2389–2397, 2020.
- [9] Y. Lv, L. Yue, Q. Li et al., "Recyclable (Fe₃O₄-NaYF₄: Yb, Tm)@TiO₂ nanocomposites with near-infrared enhanced photocatalytic activity," *Dalton Transactions*, vol. 47, no. 5, pp. 1666–1673, 2018.
- [10] W. Qin, D. Zhang, D. Zhao, L. Wang, and K. Zheng, "Near-infrared photocatalysis based on YF₃: Yb³⁺, Tm³⁺/TiO₂ core/shell nanoparticle near-infrared photocatalysis based on YF₃: Yb³⁺, Tm³⁺/TiO₂ core/shell nanoparticles," *Chemical Communications*, vol. 46, no. 13, pp. 2304–2306, 2010.
- [11] C. K. Chen, H. M. Chen, C. J. Chen, and R. S. Liu, "Plasmon-enhanced near-infrared-active materials in photoelectrochemical water splitting," *Chemical Communications*, vol. 49, no. 72, pp. 7917–7919, 2013.
- [12] L. Wang, D. D. Cui, L. Ren et al., "Boosting NIR-driven photocatalytic water splitting by constructing 2D/3D epitaxial heterostructures," *Journal of Materials Chemistry A*, vol. 7, no. 22, pp. 13629–13634, 2019.
- [13] H. C. Zhang, H. Huang, Y. Liu et al., "Porous and hollow metal-layer@SiO₂ nanocomposites as stable nanoreactors for hydrocarbon selective oxidation," *Journal of Materials Chemistry*, vol. 22, no. 38, pp. 20182–20185, 2012.
- [14] K. S. Novoselov, A. K. Geim, S. V. Morozov et al., "Electric field effect in atomically thin carbon films," *Science*, vol. 306, no. 5696, pp. 666–669, 2004.
- [15] X. Huang, Z. Yin, S. Wu et al., "Graphene-based materials: synthesis, characterization, properties, and applications," *Small*, vol. 7, no. 14, pp. 1876–1902, 2011.
- [16] J. Tian, Y. Leng, Z. Zhao et al., "Carbon quantum dots/hydrogenated TiO₂ nanobelt heterostructures and their broad spectrum photocatalytic properties under UV, visible, and near-infrared irradiation," *Nano Energy*, vol. 11, pp. 419–427, 2015.
- [17] S. Zhu, J. Zhang, S. Tang et al., "Surface chemistry routes to modulate the photoluminescence of graphene quantum dots: from fluorescence mechanism to up-conversion bioimaging applications," *Advanced Functional Materials*, vol. 22, no. 22, pp. 4732–4740, 2012.
- [18] Z. Huang, F. Lin, M. Hu et al., "Carbon dots with tunable emission, controllable size and their application for sensing hypochlorous acid," *Journal of Luminescence*, vol. 151, pp. 100–105, 2014.
- [19] K. Jiang, S. Sun, L. Zhang, Y. Wang, C. Cai, and H. Lin, "Bright-yellow-emissive N-doped carbon dots: preparation, cellular imaging, and bifunctional sensing," *ACS Applied Materials & Interfaces*, vol. 7, no. 41, pp. 23231–23238, 2015.
- [20] S. Song, B. Cheng, N. Wu, A. Meng, S. Cao, and J. Yu, "Structure effect of graphene on the photocatalytic performance of plasmonic Ag/Ag₂CO₃-rGO for photocatalytic elimination of pollutants," *Applied Catalysis B: Environmental*, vol. 181, pp. 71–78, 2016.
- [21] J. Shen, Y. Zhu, C. Chen, J. Yang, and C. Li, "Facile preparation and upconversion luminescence of graphene quantum dots," *Chemical Communications*, vol. 47, no. 9, pp. 2580–2582, 2011.
- [22] Y. Wang, Y. Zou, J. Chen, G. D. Li, and Y. Xu, "A flexible and monolithic nanocomposite aerogel of carbon nanofibers and crystalline titania: fabrication and applications," *RSC Advances*, vol. 3, no. 46, p. 3, 2013.
- [23] R. Shi, H. Li, Y. Shang et al., "Effect of nitrogen doping level on the performance of N-doped carbon quantum dot/TiO₂ composites for photocatalytic hydrogen evolution," *ChemSusChem*, vol. 10, no. 22, pp. 4650–4656, 2017.
- [24] Y. Guo, H. Li, W. Ma, W. Shi, and W. Choi, "Photocatalytic activity enhanced via surface hybridization," *Carbon Energy*, vol. 2, no. 3, pp. 308–349, 2020.
- [25] H. Yu, Y. Zhao, C. Zhou et al., "Carbon quantum dots/TiO₂ composites for efficient photocatalytic hydrogen evolution," *Journal Materials Chemistry A*, vol. 2, pp. 3344–3351, 2014.
- [26] D. Khamboonrueang, S. Srirattanapibul, I. M. Tang, and S. Thongmee, "TiO₂-rGO nanocomposite as a photo catalyst for the reduction of Cr⁶⁺," *Materials Research Bulletin*, vol. 107, pp. 236–241, 2018.
- [27] O. S. Dahham, R. Hamzah, M. A. Bakar et al., "Synthesis and structural studies of an epoxidized natural rubber/titania (ENR-50/TiO₂) hybrid under mild acid conditions," *Polymer Testing*, vol. 65, pp. 10–20, 2018.
- [28] F. Teng, G. Zhang, Y. Wang et al., "The role of carbon in the photocatalytic reaction of carbon/TiO₂ photocatalysts," *Applied Surface Science*, vol. 320, pp. 703–709, 2014.
- [29] X. Hao, Z. Jin, J. Xu, S. Min, and G. Lu, "Functionalization of TiO₂ with graphene quantum dots for efficient photocatalytic hydrogen evolution," *Superlattices and Microstructures*, vol. 94, pp. 237–244, 2016.
- [30] J. Xie, K. Huang, X. Yu et al., "Enhanced electronic properties of SnO₂ via electron transfer from graphene quantum dots for efficient perovskite solar cells," *ACS Nano*, vol. 11, no. 9, pp. 9176–9182, 2017.
- [31] L. Bao, C. Liu, Z. L. Zhang, and D. W. Pang, "Photoluminescence-tunable carbon nanodots: surface-state energy-gap tuning," *Advanced Materials*, vol. 27, no. 10, pp. 1663–1667, 2015.
- [32] H. Ding, S. B. Yu, J. S. Wei, and H. M. Xiong, "Full-color light-emitting carbon dots with a surface-state-controlled luminescence mechanism," *ACS Nano*, vol. 10, no. 1, pp. 484–491, 2016.
- [33] L. Cao, X. Wang, M. J. Mezziani et al., "Carbon dots for multiphoton bioimaging," *Journal of the American Chemical Society*, vol. 129, no. 37, pp. 11318–11319, 2007.
- [34] K. Darowicki, S. Krakowiak, and P. Ślepski, "Selection of measurement frequency in Mott-Schottky analysis of passive layer on nickel," *Electrochimica Acta*, vol. 51, pp. 2204–2208, 2007.

- [35] D. Ma, J. Zhong, J. Li, L. Wang, and R. Peng, "Enhanced photocatalytic activity of BiOCl by C70 modification and mechanism insight," *Applied Surface Science*, vol. 443, pp. 497–505, 2018.
- [36] R. P. Gupta and S. K. Sen, "Calculation of multiplet structure of corep-vacancy levels. II," *Physical Review B*, vol. 12, no. 1, pp. 15–19, 1975.
- [37] J. Kräuter, L. Mohrhuse, L. Thiedemann, M. Willms, and K. A. Shamery, "Activation of small organic molecules on Ti^{2+} -rich TiO_2 surfaces: deoxygenation vs. C–C coupling," *Zeitschrift für Naturforschung*, vol. 74, pp. 697–707, 2019.
- [38] Y. Liu, Y. F. Luo, A. A. Elzatahry et al., "Mesoporous TiO_2 mesocrystals: remarkable defects-induced crystallite-interface reactivity and their in situ conversion to single crystals," *ACS Central Science*, vol. 1, no. 7, pp. 400–408, 2015.
- [39] Y. Lu, W. J. Yin, K. L. Peng et al., "Self-hydrogenated shell promoting photocatalytic H_2 evolution on anatase TiO_2 ," *Nature Communications*, vol. 9, no. 1, p. 2752, 2018.
- [40] N. I. Zaaba, K. L. Foo, U. Hashim, S. J. Tan, W. W. Liu, and C. H. Voon, "Synthesis of graphene oxide using modified hummers method: solvent influence," *Procedia Engineering*, vol. 184, pp. 469–477, 2017.
- [41] L. Wang, Y. Y. Wan, H. Cheng et al., "Unraveling the photocatalytic water dissociation pathways on two-dimensional conjugated polymers," *Angewandte Chemie International Edition*, vol. 11, no. 24, pp. 6236–6243, 2019.
- [42] G. Wang, Y. Gong, M. Chen, and M. Zhou, "Methane activation by titanium monoxide molecules: a matrix isolation infrared spectroscopic and theoretical study," *Journal of the American Chemical Society*, vol. 128, no. 17, pp. 5974–5980, 2006.
- [43] J. S. Zhu, H. Yang, W. Zhang, Y. Mao, S. S. Lyu, and J. Chen, "An in situ raman study of intermediate adsorption engineering by high-index facet control during the hydrogen evolution reaction," *Inorganic Chemistry Frontiers*, vol. 7, no. 9, pp. 1892–1899, 2020.